Schweizerische Eidgenossenschaft
Confédération suisse
Confederazione Svizzera
Confederaziun svizra

Department of the Environment, Transport, Energy and Communication DETEC

Swiss Federal Office of Energy SFOE
Energy Research

Annual report 2017

SolAir-3

Innovative solar collectors for efficient and cost-effective solar thermal power generation – 3

Date: 22 December 2017

Town: Manno

Publisher:
Swiss Federal Office of Energy SFOE
XY Research Programme
CH-3003 Bern
www.bfe.admin.ch

Agent:
Airlight Energy Holding SA
Via Croce, 1, CH-6710 Biasca
www.airlightenergy.com

SUPSI – DTI – MEMTi
Via Cantonale, Galleria 2, CH-6928 Manno
www.supsi.ch ; www.supsi.ch/memti

ETHZ – Institute of Energy Technology
ML J 42.1, Sonneggstr. 3, CH-8092 Zurich
www.ethz.ch , www.iet.ethz.ch

Author:
Maurizio C. Barbato, SUPSI – DTI – MEMTi, maurizio.barbato@supsi.ch
Davide Montorfano, SUPSI – DTI – MEMTi, davide.montorfano@supsi.ch
Simone A. Zavattoni, SUPSI – DTI – MEMTi, simone.zavattoni@supsi.ch
Filippo Contestabile, SUPSI – DTI – MEMTi, filippo.contestabile@supsi.ch
Aldo Steinfeld, ETHZ–IET, aldo.steinfeld@ethz.ch
Andrea Pedretti, Airlight Energy Manufacturing SA, andrea.pedretti@airlightenergy.com

SFOE head of domain: Stefan Oberholzer, stefan.oberholzer@bfe.admin.ch
SFOE programme manager: Stefan Oberholzer, stefan.oberholzer@bfe.admin.ch
SFOE contract number: SI/500926-01

Swiss Federal Office of Energy SFOE
Mühlestrasse 4, CH-3063 Ittigen; postal address: CH-3003 Bern
Phone +41 58 462 56 11 · Fax +41 58 463 25 00 · contact@bfe.admin.ch · www.bfe.admin.ch

Contents

Summary

The research activities performed to date in the framework of the SolAir-3 project focuses on further analysis and characterization of the high-temperature rock-bed thermal energy storage (TES) solution proposed to be integrated in large-scale concentrating solar power (CSP) plants working with air as heat transfer fluid (Airlight Energy technology). The 100 MWh_{th} packed bed TES system of the Ait Baha CSP pilot-plant was assumed as reference for the analysis performed. A computational fluid dynamics (CFD) approach was followed to evaluate the thermo-fluid dynamics behaviour of the TES system under investigation, along with its cyclic performance, considering a total of 60 consecutive charge/discharge/idle cycles. Furthermore, a parametric analysis was also carried out with the aim of assessing the effect of some parameters, such as (i) heat transfer fluid mass flow rate during discharging and (ii) particle size distribution into the packed bed, on the overall TES performance

An important result of the CFD analysis is that a relatively weak thermal stratification into the packed bed characterizes the behaviour of the TES unit. In terms of heat transfer fluid (HTF) outflow temperature during discharging, a monotonic decrease was observed throughout the whole phase with a more pronounced reduction at the very beginning of the process indicating that the TES unit cannot provide a stable HTF outflow temperature. Conversely, an HTF outflow temperature increase during charging, up to 35°C at most above the nominal discharging temperature, was obtained; in this case also the thermocline is discharged from the beginning of the process.

The parametric analysis allowed to observe that HTF mass flow rate variation during discharging has a minor influence on the TES performance. Conversely, assuming a different particles size distribution into the packed bed allowed to obtain a slightly higher HTF discharging outflow temperature during the initial 10-15 cycles.

The performance of the TES unit was evaluated on the basis of the first- and the second-law of thermodynamics. The resulting transient performances of the TES unit showed a similar evolution increasing monotonically up to a stable value of about 90% and 88% for the energy and exergy efficiency respectively.

List of abbreviations

CFD	Computational fluid dynamics
CSP	Concentrating solar power
ORC	Organic Rankine cycle
TES	Thermal energy storage
HTF	Heat transfer fluid
HX	Heat exchanger
WHR	Waste heat recovery

Work undertaken and findings obtained

1. Ait Baha CSP pilot plant

The first industrial-scale concentrating solar power (CSP) pilot plant, based on Airlight Energy technology, has been constructed at the Cimar's site (Italcementi group) in Ait Baha (Morocco, 30.22° N, 9.15° W, altitude: 256 m) with the aim of boosting electricity production from the waste heat recovery (WHR) system of the cement factory. The CSP plant is designed to provide 3.9 MW_{th} peak to the air-to-diathermic oil heat exchanger of the organic Rankine cycle (ORC) for power generation. The power capacity of the ORC turbine, manufactured by Turboden, is 2 MWe. As visible in the aerial view of the site (figure 1), the CSP pilot plant is composed of three 211.68 m long parabolic trough collectors, leading to a total useful aperture area of 5'880 m^2, a piping system for the heat transfer fluid (HTF), air at atmospheric pressure, and a 100 MWh_{th} TES unit, based on a packed bed of rocks, to increase the plant capacity factor.

Figure 1: Aerial views of the CSP pilot plant construction site (Courtesy of Italcementi group).

The HTF enters the solar field at 270°C leaving it at 570°C. As depicted in the plant layout of figure 2, a fraction of the high-temperature HTF is fed through the TES while, the remaining part, is exploited to deliver thermal power to the air-to-oil heat exchanger for the power block. The TES unit is designed for daily operating conditions of 10 h of charging followed by 4.5 h of discharging and 9.5 h of idle. To effectively store the resulting amount of thermal energy, a total volume of 381.2 m^3 of sedimentary rocks were positioned into the truncated cone shaped TES tank. The lateral walls of the TES tank consist of a first layer of ultra-high performance concrete with high mechanical stability, in direct contact with the packed bed of rocks, followed by a thicker layer of low-density concrete with a low thermal conductivity. The TES unit is buried in order to exploit the surrounding ground for structural purposes. To minimize heat losses, the TES tank is insulated with Foamglas® and Microtherm® on both the lateral walls and under the lid. The main characteristics of the packed bed, along with the reference operating conditions of the TES unit, are reported in table 1 and table 2.

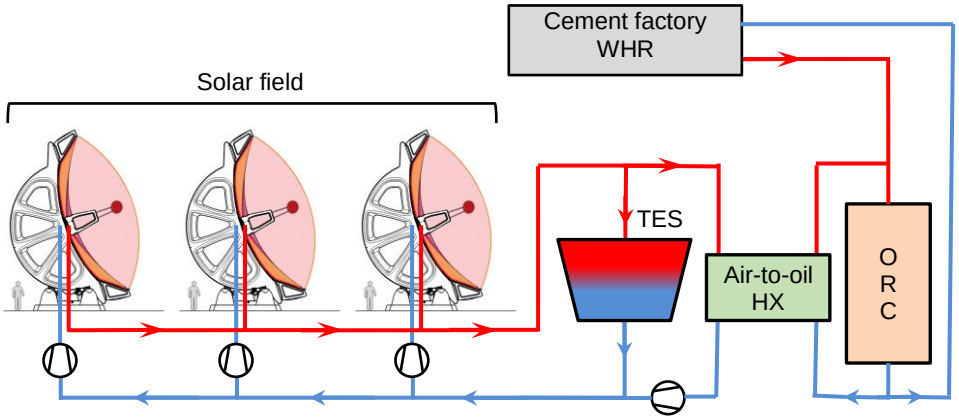

Figure 2: Ait Baha CSP pilot plant layout.

Packed bed		
upper diameter	12	[m]
lower diameter	10	[m]
height	4	[m]
rocks average diameter	0.03	[m]

Table 1: Packed bed characteristics of the Ait Baha TES unit.

TES unit operating conditions		
Charging		
temperature	570	[°C]
HTF mass flow rate	1.72	[kg/s]
nominal duration	10	[h]
Discharging		
temperature	270	[°C]
HTF mass flow rate	4.06	[kg/s]
nominal duration	4.5	[h]
Idle		
HTF mass flow rate	0	[kg/s]
nominal duration	9.5	[h]

Table 2: Reference operating conditions of the Ait Baha TES unit.

1.1. CFD model, boundary conditions and numerical details

For evaluating the transient performance of the TES unit under investigation, a computational fluid dynamics approach was followed. Details on the modelling approach and validation can be found in ref [1]. The geometric characteristics of the TES unit were exploited to minimize the computational domain; therefore, starting from the original 3D CAD model (l.h.s. of Figure 3), a 2D axisymmetric computational domain was extracted and the relative computational grid was generated. A mesh sensitivity analysis was performed showing the independency of the results with a grid of 92’500 elements.

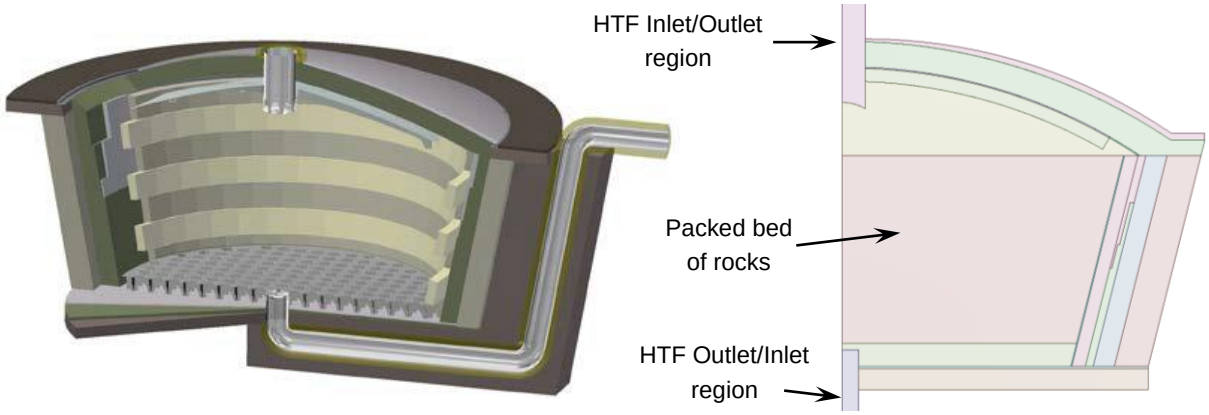

Figure 3: Ait Baha TES unit: 3D CAD model [2] and 2D axisymmetric computational domain.

The CFD model developed solves mass, momentum, energy, turbulent kinetic energy and turbulent dissipation rate, transport equations by means of Fluent 17.1 code from ANSYS. Turbulence effects were accounted for by means of the realizable *k-ε* model [3] with enhanced wall treatment, as near-wall modelling method [4]. To determine the flow regime into the rocks, its permeability *K* was selected as characteristic length in the definition of the Reynolds number Re_K [5]:

$$Re_K = \frac{v_{sup} \cdot \rho_f \cdot K^{0.5}}{\mu} \quad (1)$$

The transition from laminar to turbulent regimen occurs when Re_K is in the order of 100. Since for the reference operating conditions of the TES unit under investigation (table 2) the value of Re_K is well below this threshold, a laminar region is modeled into the packed bed.

The TES unit is charged form top and discharged from the bottom therefore, mass flow inlet and pressure outlet BCs were applied on the upper and the lower duct respectively to model charge phase. Conversely, the discharge phase was modeled by reversing the HTF inflow and outflow BCs: mass flow inlet and pressure outlet BCs were specified at the lower and at the upper duct respectively. The third and final process of each cycle is the idle phase. The latter was modeled by applying a wall BC, i.e. none HTF flow through the TES unit, to both the upper and the lower ducts. The inlet BC, during charging and discharging, was specified with constant values of mass flow rate and temperature according to the operating conditions of the TES unit.

As previously mentioned, the TES unit containing tank is made of two different kinds of concrete, high-performance concrete, in direct contact with the packed bed of rocks, and low density concrete, to ensure proper structural stability and thermal performance. Concerning the latter, a sandwich of two different insulating materials (Microtherm® and Foamglas®) is exploited to minimize the heat losses.

Thermal energy losses by means of conduction through the ground and convection/radiation from the lid towards the environment were accounted for assuming a constant soil temperature boundary condition (BC), 1 m apart from the lateral and bottom TES walls, for the former and a mixed convection/radiation BC for the latter.

The packed bed of natural rocks was considered as a continuum and hence it was modelled exploiting the porous media approach [5]. Local thermal equilibrium (LTE model) between the solid matrix and the fluid phase was assumed; therefore, a single conservation equation of energy is solved to model the heat transfer through the porous medium:

$$\frac{\partial}{\partial t}\left(\varepsilon \cdot \rho_f \cdot E_f + (1-\varepsilon) \cdot \rho_s \cdot E_s\right) + \nabla \cdot \left(\vec{v} \cdot \left(\rho_f \cdot E_f + p\right)\right) = \nabla \cdot \left(k_{eff} \cdot \nabla T\right) \quad (2)$$

The diffusive term on the r.h.s. of eq. (2) is characterized by an effective thermal conductivity (k_{eff}) of the porous medium. In the simplest form, it can be computed as a porosity-weighted average of the thermal conductivities of the solid and the fluid phases respectively. However, more sophisticated effective thermal conductivity formulations allow to consider the effect of several heat transfer phenomena occurring into the system. This is the case of the effective thermal conductivity considered for the present study, based upon the Kunii & Smith's model [6, 7], which allows to account for all the conductive-driven and radiative-driven heat transfer mechanisms occurring into the packed bed.

A quadratic void fraction distribution, varying from 0.325 at the bottom up to 0.37 at the top of the packed bed, was implemented in order to replicate the thickness effect. Conversely, the effect of channeling was considered negligible since the characteristic ratio of vessel diameter over particle diameter (d_{vessel}/d_p) is well above the suggested threshold value of 25-30 [8, 9].

Temperature dependent properties of air and solid materials (concretes and insulating materials) were modelled as piecewise linear interpolations of tabulated data [10] and manufacturers datasheets respectively.

All the model equations were solved with second order accurate numerical schemes [11]. The pressure-implicit with splitting of operators (PISO) algorithm and the pressure staggering option (PRESTO!) scheme were used to couple the velocity and pressure fields and to solve the pressure-correction equation. Convergence was considered achieved when mass, momentum and turbulence residuals were below 10^{-5} and energy residual was below 10^{-8}.

1.2. TES performance evaluation

The TES performance was evaluated, for each cycle, on the basis of an energy and an exergy efficiency index based on the first- and the second-law of thermodynamics respectively. The energy efficiency is defined as the ratio of the net thermal energy recovered during discharging divided by the net thermal energy input during charging:

$$\eta_I = \frac{\int_0^{t_{dis.}} \dot{m}_{HTF,dis.}\left(h_{top} - h_{bott.}\right)dt}{\int_0^{t_{ch.}} \dot{m}_{HTF,ch.}\left(h_{top} - h_{bott.}\right)dt} \qquad (3)$$

where $\dot{m}$ [kg/s] is the HTF mass flow rate and h [J/kg] the specific enthalpy of the HTF, evaluated at the upper (top) and at the lower ($bott.$) sections of the TES unit, during charging ($ch.$) and discharging ($dis.$) respectively. Similarly, the exergy efficiency is defined as the ratio of the net exergy recovered during discharging divided by the net exergy input during charging. In the equation, T_{ref} [K] is the reference absolute temperature (293 K) and s [J/(kg·K)] the specific entropy of the HTF.

$$\eta_{II} = \frac{\int_0^{t_{dis.}} \dot{m}_{HTF,dis.}\left[\left(h_{top} - h_{bott.}\right) - T_{ref}\left(s_{top} - s_{bott.}\right)\right]dt}{\int_0^{t_{ch.}} \dot{m}_{HTF,ch.}\left[\left(h_{top} - h_{bott.}\right) - T_{ref}\left(s_{top} - s_{bott.}\right)\right]dt} \qquad (4)$$

The specific entropy variation, during charging and discharging, was calculated, assuming the HTF as an ideal gas, with the following equation:

$$s_{top} - s_{bott.} = \bar{c}_p \, ln\frac{T_{top}}{T_{bott.}} - R \, ln\frac{p_{top}}{p_{bott.}} \qquad (5)$$

where $\bar{c}_p$ [J/(kg·K)] is the HTF specific heat evaluated at the average temperature between T_{top} and $T_{bott.}$ while R [J/(kg·K)] is the gas constant and p_{top} .[Pa] and $p_{bott.}$ [Pa] correspond to the absolute HTF pressure in the upper and lower regions of the tank respectively.

1.3. Ait Baha TES cyclic performance analysis

The Ait Baha TES unit was analysed by simulating 60 consecutive charging/discharging/idle cycles according to the operating conditions reported in table 2. At the beginning of the numerical simulation the TES unit was assumed to be in thermal equilibrium with the environment (20°C). Before starting with the cyclic operation, a total of 5 consecutive pre-charging cycles (10 h charging and 14 h idle) were assumed with the aim of reducing the time required by the TES to achieve a stable thermal stratification into the packed bed [12]. Another important aspect of the cyclic operation of the TES unit is related to the discharging. According to the operating conditions (table 2), the nominal duration is 4.5 h but, in the real TES operation, the discharging duration is governed by the HTF outflow temperature which, for an efficient TES integration into the pilot-plant, cannot decrease by more than 40-45°C from the nominal charging temperature. Therefore, the discharging duration lasts as long as the HTF outflow temperature constraint is verified and anyway no longer than 4.5 h (nominal discharging duration).

According to the simulation results, the temperature constraint was achieved after 4 h of discharging; as a consequence, the duration of the idle phase was extended to 10 h. Figure 4 shows the evolution of the HTF outflow non-dimensional temperature at the end of all the charge (red squares) and discharge (blue squares) phases analysed. The non-dimensional temperature is obtained dividing the resulting HTF outflow temperature by the nominal charging or discharging temperature. Concerning the charging phases the simulations results show that that during the first 10 cycles, the final HTF outflow temperature is lower than the nominal discharging temperature. For all the consecutive cycles, a partial discharge of the thermocline is observed with the non-dimensional final HTF outflow temperature approaching asymptotically the value of 1.13. Conversely, the final HTF outflow temperature during discharging showed a more pronounced variation with a rapid decrease down to the minimum of about 0.917 at the end of the 12^{th} cycle. From this point forward, the non-dimensional HTF outflow temperature increases approaching asymptotically the value of 0.93 once a stable thermal stratification into the packed bed is achieved.

Figure 5 shows the transient evolution of the HTF outflow temperature during some of all the discharge phases analysed. An important consideration that can be drawn from the simulation results is that the HTF outflow temperature decreases monotonically throughout the whole discharge phase with a more pronounced reduction at the very beginning of the process. This indicates that, despite the 10 h of charging, the average temperature of the upper layers of the packed bed is lower than the charging temperature and therefore the TES unit cannot provide a stable HTF outflow temperature since the thermocline is discharged from the beginning of the process.

The resulting performance of the TES unit, evaluated according to the first law (eq. 3) and the second law (eq. 4) of thermodynamics, are summarized in figure 6. Green dots and purple squares indicate the cycle's energy and exergy efficiency respectively; however, it has to be mentioned that, for the performance evaluation of the TES system, the thermal energy stored during pre-charging is not accounted for. The resulting transient performance of the TES unit show a similar evolution increasing monotonically from 0.52 and 0.63, for the first cycle, up to a stable value of about 0.9 and 0.88, after the 60^{th} cycle, for the energy and exergy efficiency respectively. An interesting point is that, thanks to pre-charging, the exergy efficiency is higher than the energy efficiency for the first 4 cycles while, from the 6^{th} cycle the behaviour is reversed. From a graphical standpoint, a comparison between the temperature contours of the TES unit during the 1^{st} cycle (l.h.s of the figures) and the 60^{th} cycle (r.h.s. of the figures) is reported in figure 7. According to the simulations results, it can be observed that the thermocline zone spreads over the whole packed bed height from the 1^{st} cycle indicating a relatively weak thermal stratification and hence a reduced thermodynamic quality of the energy stored, i.e. lower exergy stored. Focusing on the temperature contours at the end of discharging (figure 7b), strong temperature gradient in the radial direction can be observed in the bottom region of the packed bed due to the geometry of the HTF distributor of the lower duct. At the end of the idle phase (figure 7c), the combined action of heat losses and internal heat transfer mechanisms lead to a slightly reduction of the average temperature of the packed bed and to a mitigation of the radial temperature gradients. Once a stable thermal stratification into the packed bed is reached, the pressure drop through the TES unit is about 45 Pa and 158 Pa for the charging and the discharging respectively. The heat losses

resulted to increase with time stabilizing in the order of 10% at most of the net thermal energy input during charging. According to the simulation results, the major contribution of heat losses can be attributed to the lid in the upper region of the TES unit (60% of the total heat losses) followed by the lateral walls (20%) and the basement (20%).

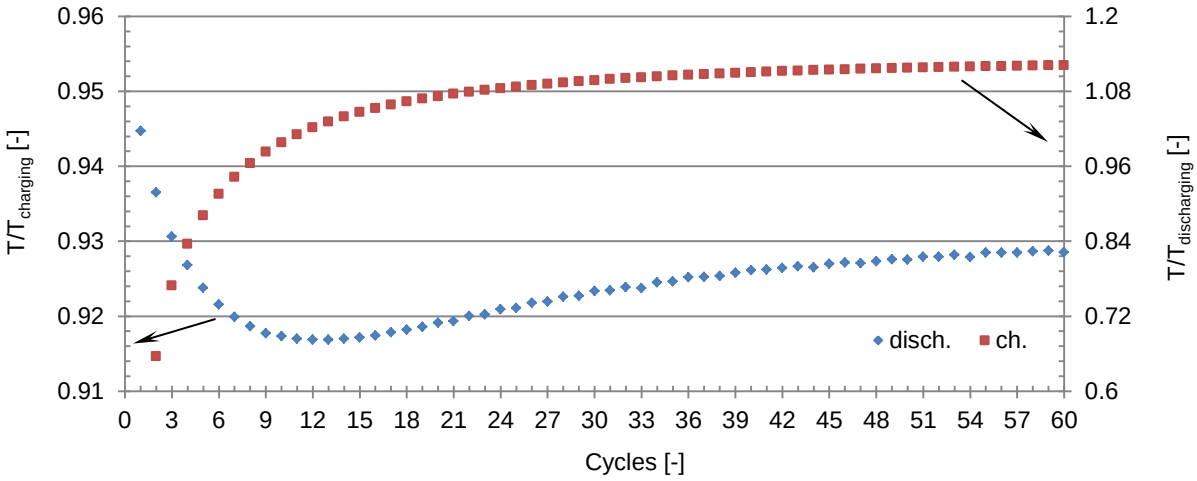

Figure 4: Non-dimensional final HTF outflow temperature of charging (red squares) and discharging (blue squares).

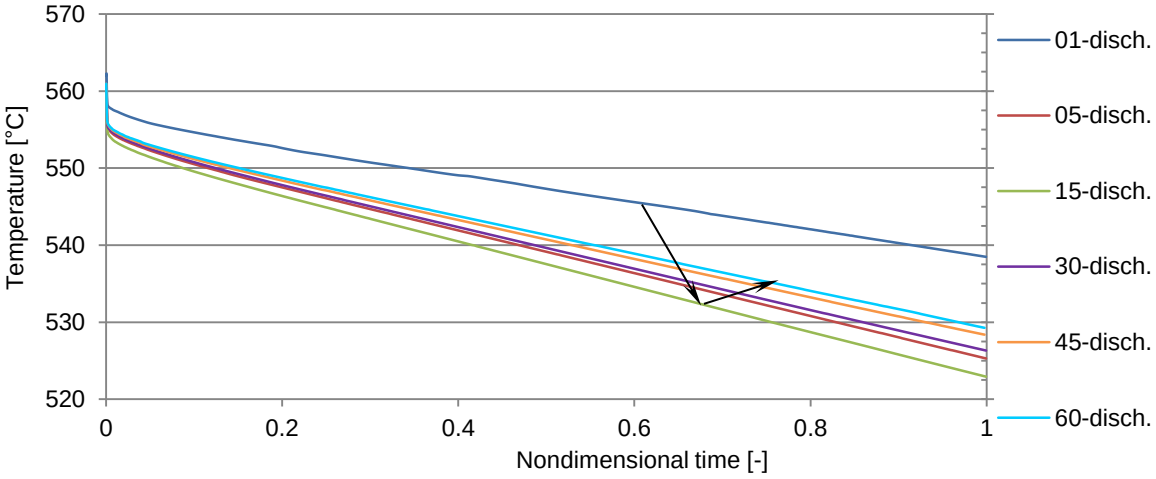

Figure 5: Transient HTF outflow temperature during some of the discharge phases simulated.

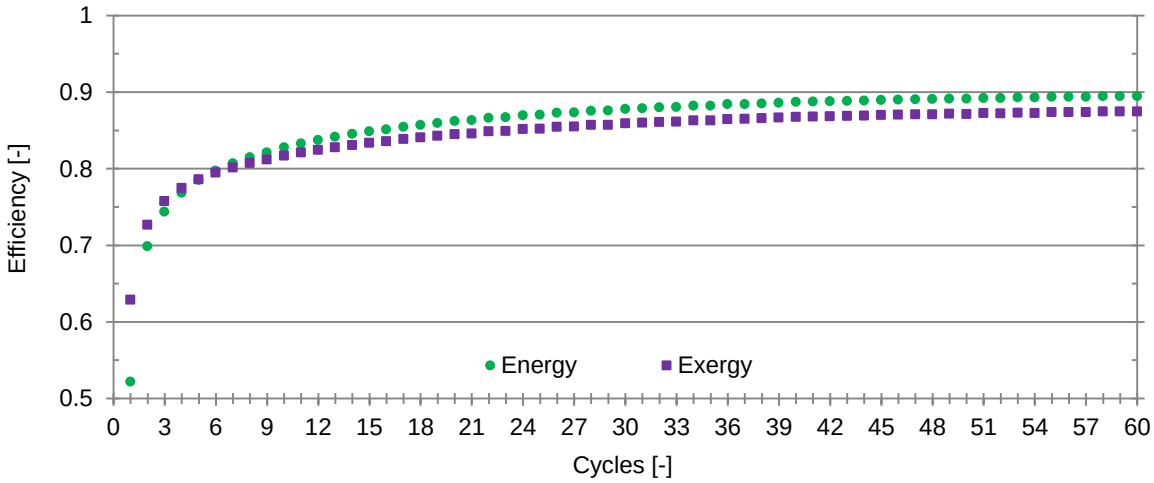

Figure 6: Performance of the Ait Baha TES unit: Energy (green dots) and exergy (purple squares) efficiencies.

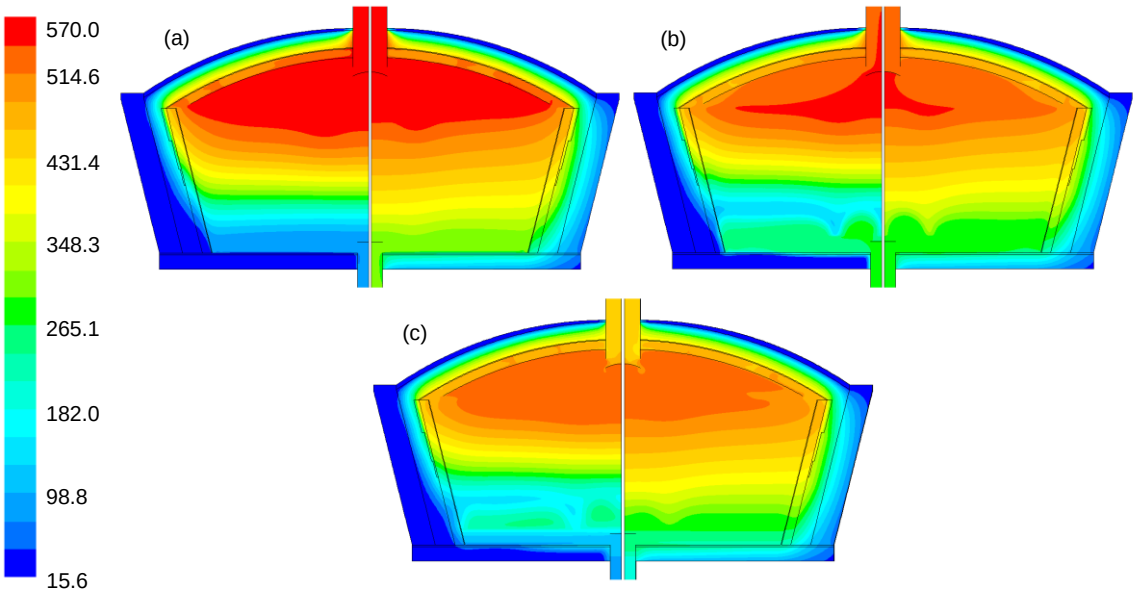

Figure 7: Comparison of the TES unit temperature contours at the end of the 1st (l.h.s) and the 60th (r.h.s.) charge (a), discharge (b) and idle (c) processes. Temperature values [°C].

1.4. Ait Baha TES parametric analysis

Once characterized the thermo-fluid dynamics behaviour of the Ait Baha TES unit, operating under reference conditions (table 2), the focus of the study was shifted towards a parametric analysis with the aim of evaluating the effect of some parameters on the TES unit cyclic performance. The two parameters investigated are: (i) the discharging HTF mass flow rate and (ii) the particles size distribution into the packed bed.

1.4.1. Effect of HTF discharging mass flow rate on the TES performance

According to the reference operating conditions of the Ait Baha pilot plant TES unit, the HTF mass flow rate during discharging is much larger than the one during charging leading therefore to higher velocity of the HTF trough the packed bed at the expanses of a larger pressure drop and therefore higher pumping power. The aim of this analysis is to evaluate the effect that the amount of HTF mass flow rate during discharging has on the overall TES performance on the basis of the first- and the second-law of thermodynamics (eq. 4). Concerning the former, to account also for the pumping power required to complete the cycles, it was redefined differently:

$$\eta_I = \frac{\int_0^{t_{dis.}} \dot{m}_{HTF,dis.}\left(h_{top} - h_{bott.}\right)dt}{\int_0^{t_{ch.}} \dot{m}_{HTF,ch.}\left(h_{top} - h_{bott.}\right)dt + \int_0^{t_{ch.}} \frac{\dot{m}_{HTF,ch.}\Delta p}{\rho_f \cdot \eta_{fan} \cdot \eta_{Rankine}}\,dt + \int_0^{t_{dis.}} \frac{\dot{m}_{HTF,dis.}\Delta p}{\rho_f \cdot \eta_{fan} \cdot \eta_{Rankine}}\,dt} \quad (6)$$

where ρ_f indicates the HTF density evaluated at discharging temperature; η_{fan} indicates the efficiency of the fan (0.95) exploited to keep the HTF flowing; $\eta_{Rankine}$ is the efficiency of the Rankine cycle (0.3) to produce the electricity needed by the fan, and Δp is the pressure drop between inlet and outlet sections of the TES unit.

Three different cases where simulated keeping unchanged all the TES reference operating conditions except the HTF mass flow rate during discharging and, as a consequence, the duration of the discharging phase. Table 3 provides an overview of the three cases analysed.

	HTF discharging mass flow rate [kg/s]	**Discharging duration [h]**
Case-1	1.72	9
Case-2	2.89	5.5
Case-3	5.23	3

Table 3: HTF discharging mass flow rate, and relative duration, of the three cases analysed.

1.4.2. Results and discussion

The same CFD modelling approach, detailed in paragraph 1.1, was applied to evaluate both the thermo-fluid dynamics behaviour and the performance of the TES unit subjected to different HTF mass flow rate during discharging. The TES unit was analysed by simulating 50 consecutive charging/discharging/idle cycles with a total of 5 consecutive pre-charging cycles (10 h charging and 14 h idle).

Figure 8 shows the resulting transient evolution of the HTF outflow temperature during discharging of the three cases analysed. According to the results obtained, the variation of the HTF discharging mass flow rate in the range considered, has minor influence on HTF outflow temperature during discharging. Nevertheless, a different transient evolution of the discharging HTF outflow temperature can be observed at the very beginning of the process (between the non-dimensional time of 0 and 0.02): reducing the HTF mass flow rate leads to a less pronounced decrease of the discharging outflow temperature.

The performance of the TES unit were also evaluated according to the first- (eq. 6) and the second-law of thermodynamics (eq. 4) obtaining the results reported in figure 9 and figure 10 respectively. Both the indexes for all the cases analysed follow the same evolution: a monotonically increase thorough all the cycles, with a sharper rate during the first 5-10 cycles, up to the achievement of a stable thermal stratification into the packed bed. According to the results obtained, case-2 seems to perform slightly better than case-1 and case-3 in spite of being in between the two in terms of HTF mass flow rate. This result can be attributed to the fact that in case-2, the duration of the discharging phase was rather too long (as demonstrated by the 3°C lower HTF outflow temperature at the end of discharging) leading to a slightly higher amount of energy and exergy recovered. However, an important consideration that can be drawn from these results is that, the effect of varying the HTF mass flow rate in the range considered for the analysis, has a minor influence also from the performance point of view. Small differences can be observed during the first cycles but, when a stable thermal stratification into the packed bed is achieved, the performance of the TES unit are not affected by the variation of the HTF discharging mass flow rate.

Even at the highest HTF discharging mass flow rate considered, the thermal-equivalent pumping power resulted to be very small in comparison to the net incoming thermal power into the TES unit during charging. Once a stable thermal stratification into the packed bed was achieved, the pumping power was in the order of 0.14%, 0.22% and 0.5% with respect to the net input power during charging for case-1, case-2 and case-3 respectively.

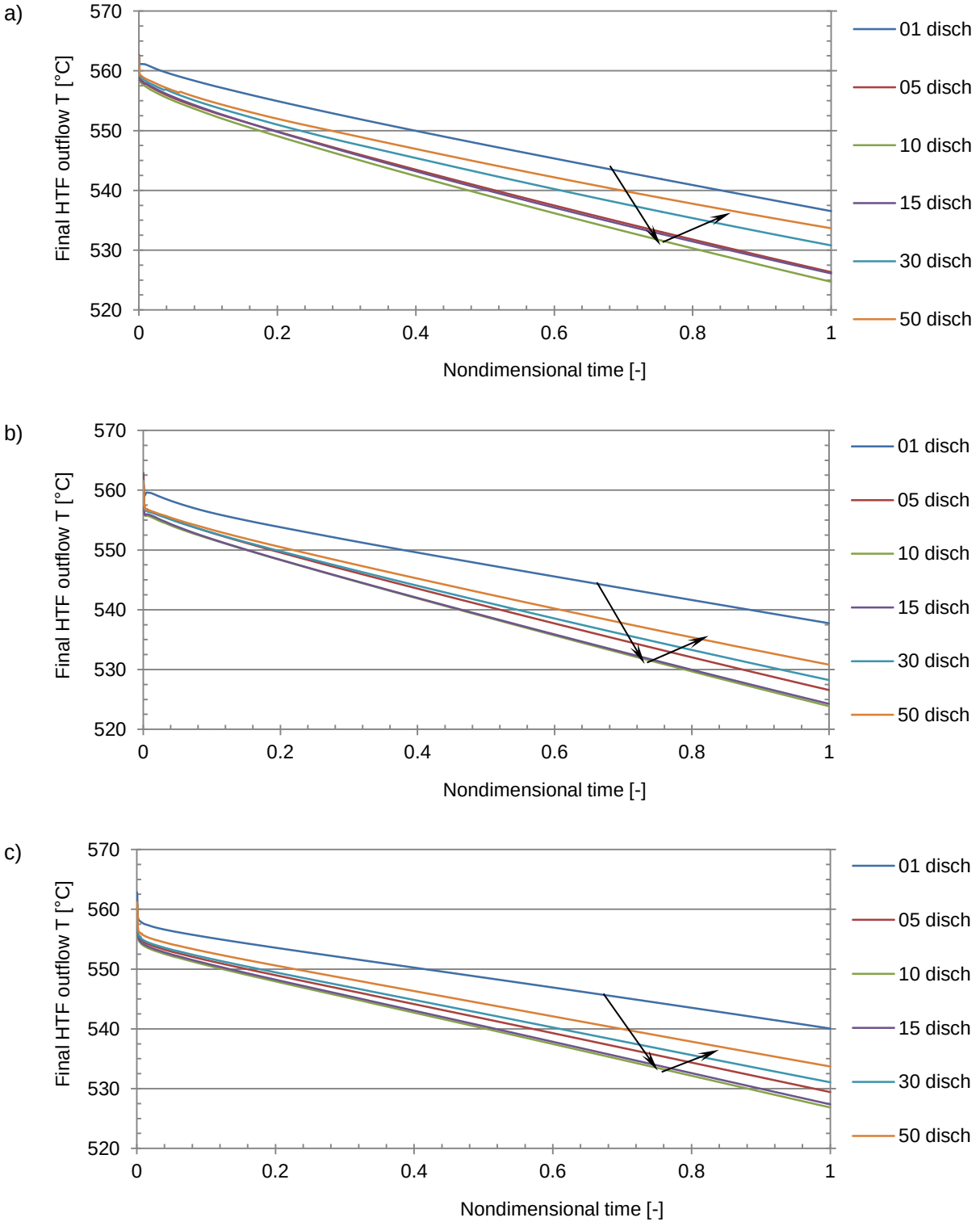

Figure 8: Comparison between the transient HTF outflow temperature during discharging for the three cases analysed: a) Case-1, b) Case-2 and c) Case-3.

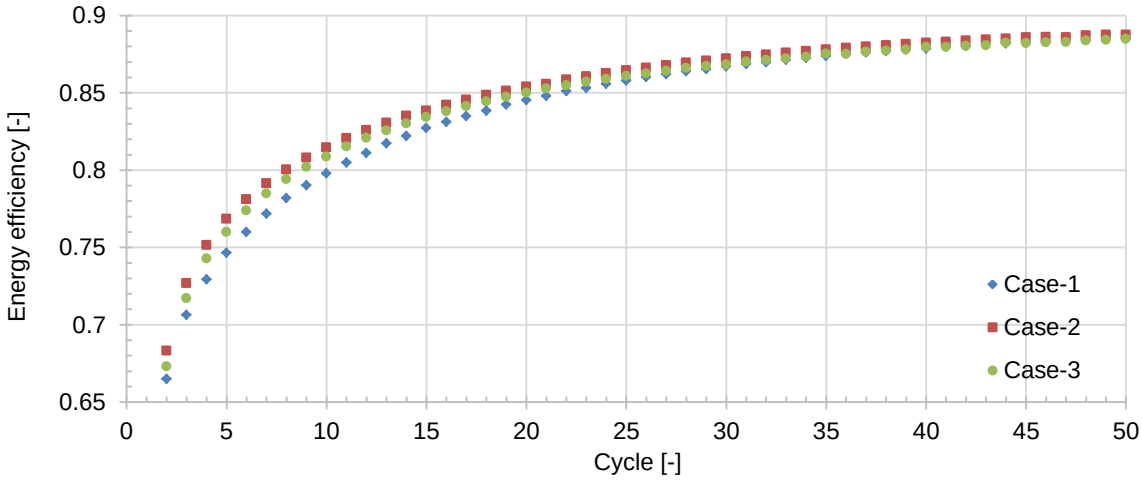

Figure 9: Comparison between the resulting energy efficiency (eq. 6) of the three cases analysed.

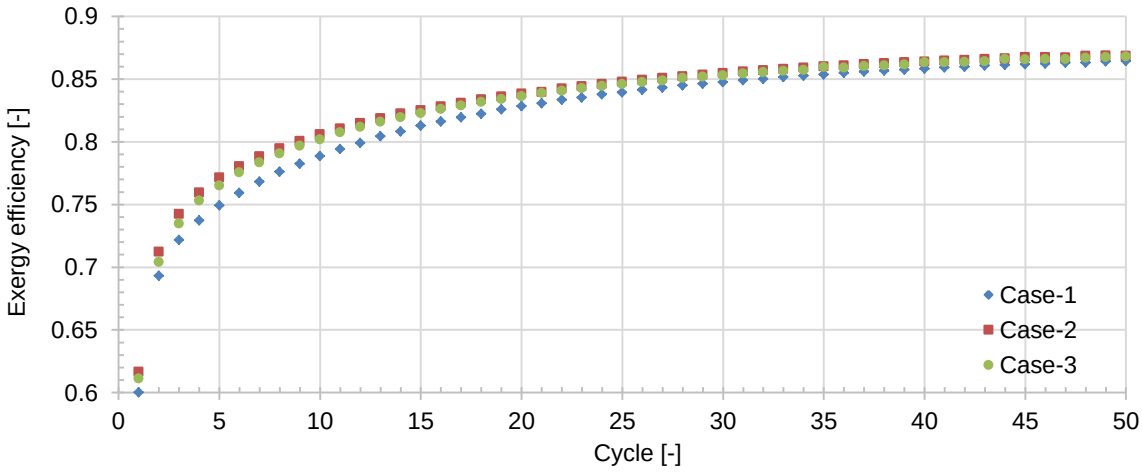

Figure 10: Comparison between the resulting exergy efficiency (eq. 4) of the three cases analysed.

1.4.3. Effect of packed bed particle size distribution on the TES performance

In this paragraph, the effect of varying the particle size distribution on the performance of the TES unit was investigated. A non-uniform particles distribution into the TES unit, characterized by a lower diameters of the particles in the first meter of the packed bed upper region, was proposed and compared with the original configuration (homogeneous particles with 0.03 m average diameter). Figure 11 shows a schematic representation of the reference case of the Ait Baha TES unit along with the TES unit with a different particles size distribution (case-4). In the figures, the borders of the packed bed are highlighted by the red lines.

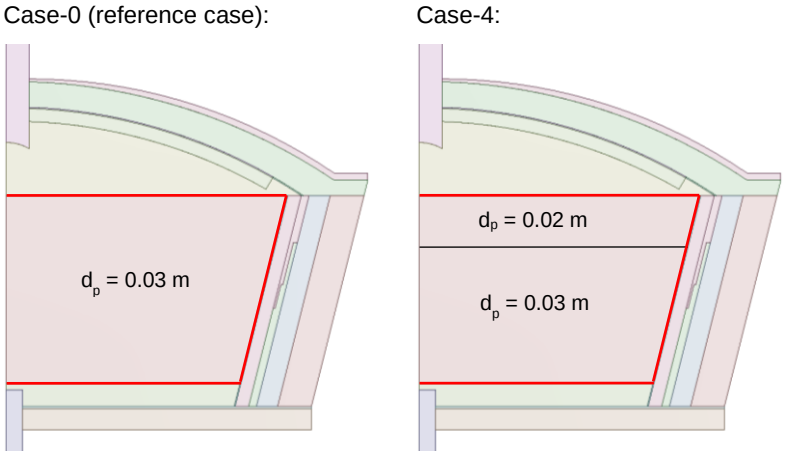

Figure 11: Schematic of the particle size distribution into the reference packed bed (case-0) along with the different particles size distribution proposed (case-4).

According to the CFD simulations results, the transient evolution of the HTF outflow temperature during discharging (figure 12) is still characterized by a monotonic decrease with a sharp reduction at the very beginning of the process as already observed from the simulations results of the reference case (figure 5). However, looking at the comparison between the final HTF outflow temperature during discharging for case-0 and case-4 (figure 13) it can be observed that in the case of non-uniform particles size distribution, a slightly higher HTF outflow temperature can be obtained especially during the initial 15-20 cycles. Once a stable thermal stratification into the packed bed is achieved, the HTF outflow temperature of the two cases is almost the same.

Figure 14 shows the comparison between the performance of the TES unit with non-uniform particle size distribution into the packed bed, along with those of the reference case, evaluated according to the first- (eq. 6) and the second-law of thermodynamics (eq. 4). Also from the performance point of view, being directly related to the HTF outflow temperature, the same conclusions can be drawn: a slightly higher values of energy and exergy efficiencies can be observed during the initial 15-20 cycles but almost the same performance should be expected between the two cases once a stable thermal stratification into the packed bed is achieved. From a graphical point of view, figure 15 shows the comparison between the temperature contours of the TES system at the end of the first, the tenth and the thirtieth discharging phase for case-0 (l.h.s.) and case-4 (r.h.s.). The effect of the different particle size distribution is more visible during the initial cycles because the TES unit is largely oversized for the expected working cycle and only at start-up a large amount of thermal energy is stored into the packed bed with the 5 pre-charging assumed. The thermal energy stored during pre-charging is then partially recovered during consecutive discharging leading to the development of a wide thermocline throughout all the packed bed height and therefore mitigating the effect of a non-uniform particle size distribution into the packed bed.

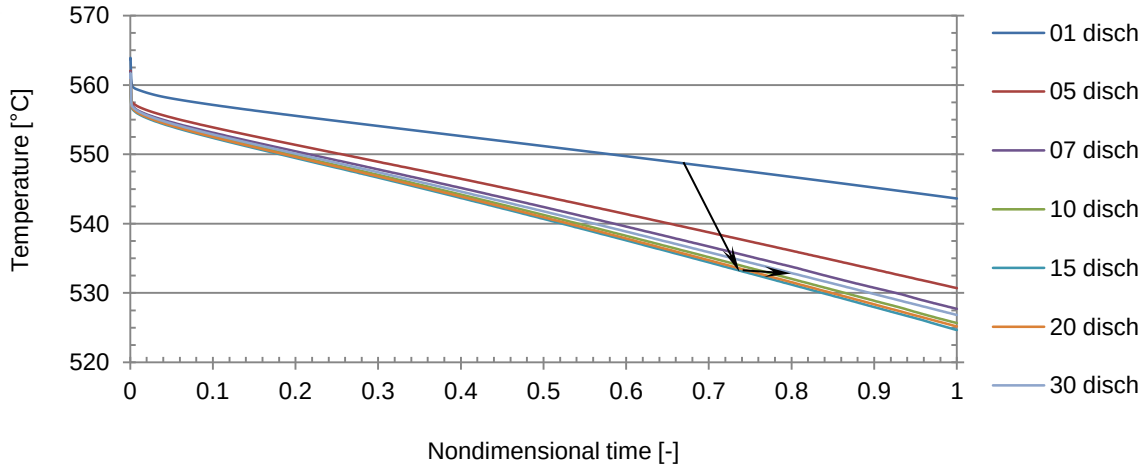

Figure 12: Case-4: transient HTF outflow temperature during some of the discharge phases simulated.

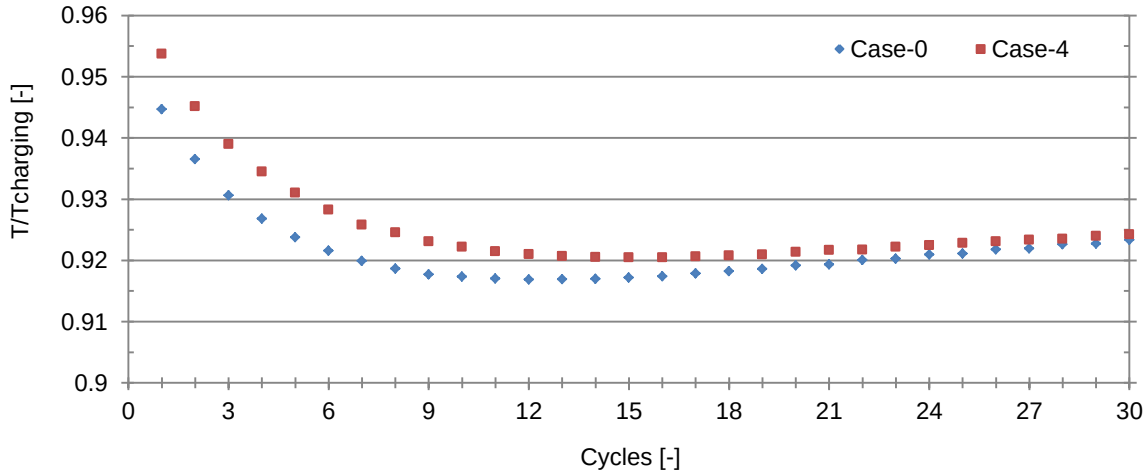

Figure 13: Comparison between the resulting final HTF non-dimension outflow temperature of case-0 (reference TES unit) and case-4 (non-uniform particles size distribution into the packed bed).

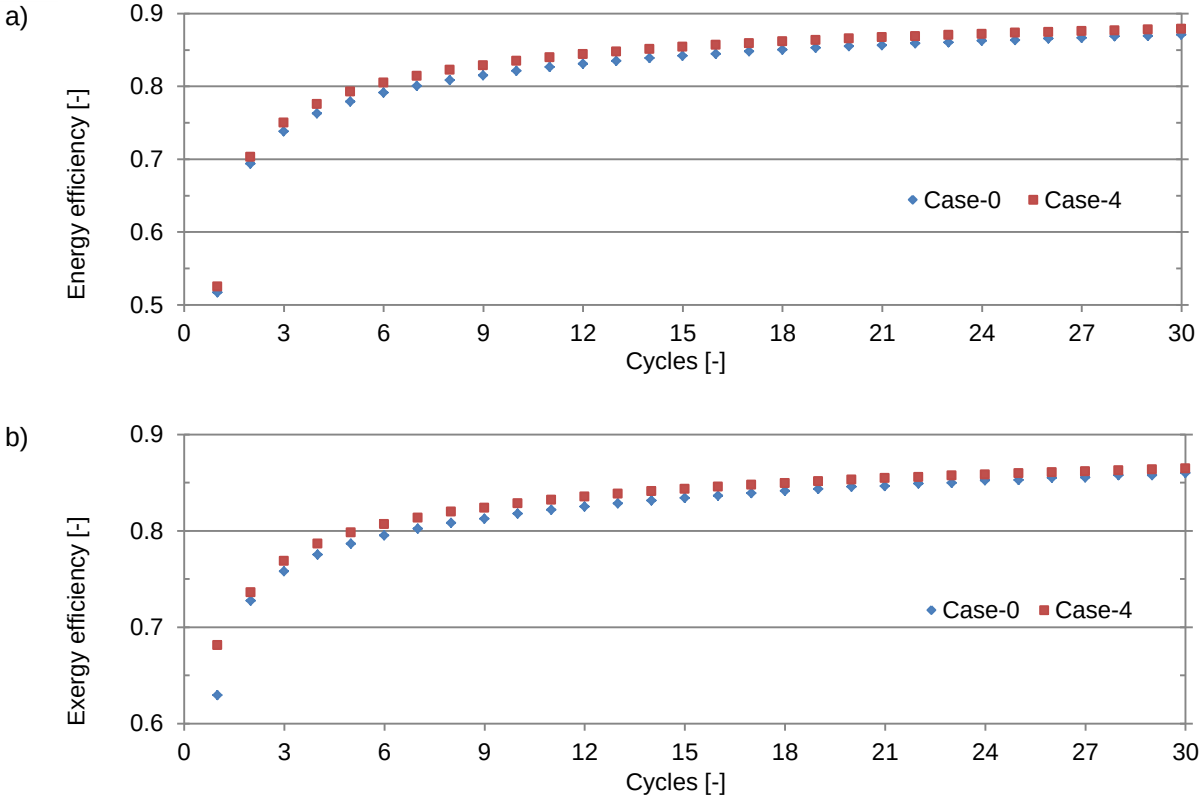

Figure 14: Comparison between the performance of the reference TES unit (case-0) and case-4: a) energy efficiency (eq. 6); b) exergy efficiency (eq. 4).

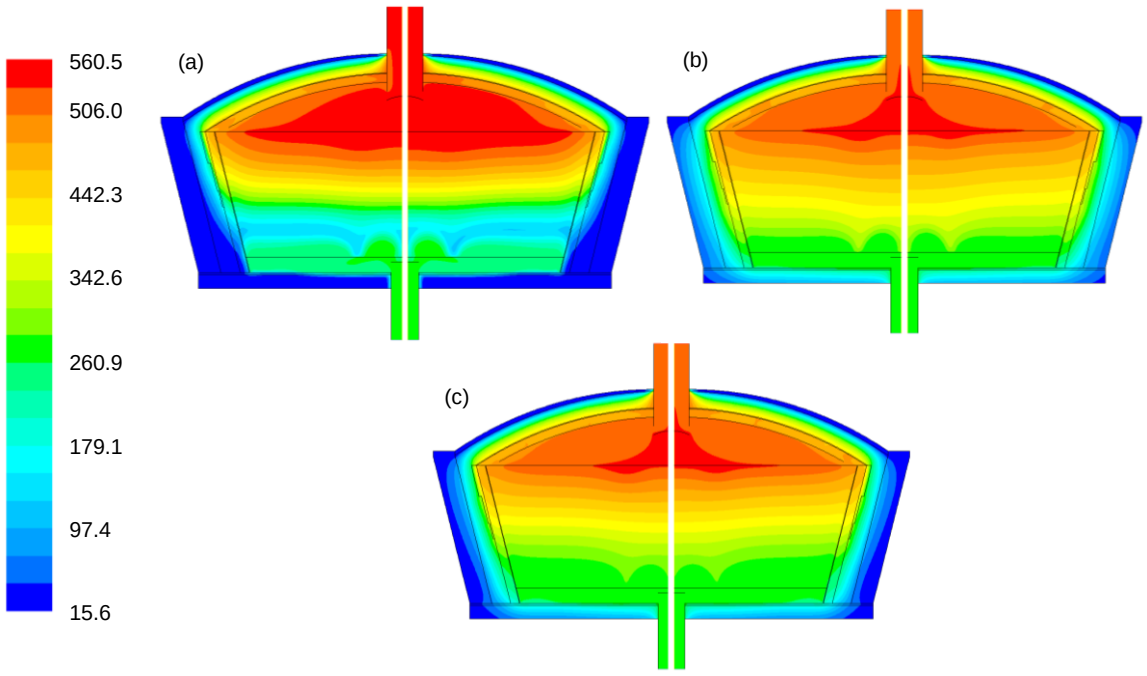

Figure 15: Comparison of the TES unit temperature contours for case-0 (l.h.s.) and case-4 (r.h.s.) at the end of the (a) 1st, (b) the 10th and (c) the 30th discharging. Temperature values [°C].

1.5. Summary and conclusions

The thermo-fluid dynamics behaviour of the packed bed TES system integrated in the Ait Baha pilot plant was evaluated exploiting a 2D CFD-based approach. The TES unit was analysed under 60 consecutive cycles of 10 h charging followed by 4 h discharging, with higher HTF mass flow rate, and 10 h of idle. The real discharging duration of 4 h was determined by the HTF outflow temperature which, for an efficient integration into the pilot plant, cannot be reduced by more than 40-45°C with respect to the nominal charging temperature of 570°C. Since at the beginning of the simulation the TES unit was considered to be in thermal equilibrium with the environment, a total of 5 pre-charging cycles were assumed prior to the cyclic operation to reduce the initial transients. Furthermore, a parametric analysis was also performed with the aim of assessing the effect of parameters, such as (i) HTF discharging mass flow rate and (ii) particle size distribution into the packed bed, have on the overall TES cyclic performance.

An important result of the simulation is that a relatively weak thermal stratification into the packed bed characterizes the behaviour of the TES unit. In terms of HTF outflow temperature during discharging, a monotonic decrease was observed throughout the whole phase with a more pronounced reduction at the very beginning of the process indicating that the TES unit cannot provide a stable HTF outflow temperature. Conversely, an HTF outflow temperature increase during charging, up to 35°C at most above the nominal discharging temperature, was obtained; in this case also the thermocline is discharged from the beginning of the process.

The parametric analysis allowed to observe that HTF mass flow rate variation during discharging has a minor influence on the TES performance. Conversely, assuming a different particles size distribution into the packed bed allowed to obtain a slightly higher HTF discharging outflow temperature during the initial 10-15 cycles.

The performance of the TES unit was evaluated on the basis of the first- and the second-law of thermodynamics. The resulting transient performances of the TES unit showed a similar evolution increasing monotonically up to a stable value of about 90% and 88% for the energy and exergy efficiency respectively.

2. Publications

The results of this work have partially been published at the 23rd Solar Power and Chemical Energy Systems (SolarPACES) conference, held in Santiago Chile on September 26th – 29th 2017, through an oral presentation, along with the accompanying paper titled:

Simone A. Zavattoni, Giw Zanganeh, Andrea Pedretti, Maurizio C. Barbato, "Numerical analysis of the packed bed TES systems integrated into the first parabolic trough CSP pilot-plant using air as heat transfer fluid".

3. References

[1] S. Zavattoni, M. Barbato, A. Pedretti, G. Zanganeh and A. Steinfeld, "Effective thermal conductivity and axial porosity distribution of a rock-bed TES system: CFD modeling and experimental validation," in *SolarPACES Conference Proceedings*, Marrakech, Morocco, 2012.

[2] G. Zanganeh, A. Pedretti, S. Zavattoni, M. Barbato, A. Haselbacher and A. Steinfeld, "Design of a 100 MWhth packed-bed thermal energy storage," *Energy Procedia,* vol. 49, pp. 1071-1077, 2014.

[3] T. Shih, W. Liou, A. Shabbir, Z. Yang and J. Zhu, "A new k-epsilon eddy viscosity model for high Reynolds number turbulent flows - Model development and validation," *Computers and Fluids,* vol. 24, no. 3, pp. 227-283, 1995.

[4] J. Tu, G. Yeoh and C. Liu, Computational Fluid Dynamics - A Practical Approach, USA: Elsevier Inc., 2008.

[5] D. Nield and A. Bejan, Convection in porous media - Third edition, USA: Springer, 2006.

[6] S. Yagi and D. Kunii, "Studies on effective thermal conductivities in packed beds," *A.I.Ch.E. Journal,* vol. 3, no. 3, pp. 373-381, 1957.

[7] D. Kunii and J. Smith, “Heat transfer characteristics of porous rocks,” *A.I.Ch.E. Journal,* vol. 6, no. 1, pp. 71-78, 1960.

[8] D. Beasley and J. Clark, “Transient response of a packed bed for thermal energy storage,” *International Journal of Heat and Mass Transfer,* vol. 27, no. 9, pp. 1659-1669, 1984.

[9] A. Ribeiro, P. Neto and C. Pinho, “Mean porosity and pressure drop measurements in packed beds of monosized spheres: Side wall effect,” *International Review of Chemical Engineering,* vol. 2, no. 1, pp. 40-46, 2010.

[10] F. P. Incropera, D. Dewitt, T. Bergman and A. Lavine, Fundamentals of heat and mass transfer, 6th edition, John Wiley & Sons, 2007.

[11] H. Versteeg and W. Malalasekera, An introduction to computational fluid dynamics: the finite volume method approach, Harlow, England: Longman Scientific and Technical, 1995.

[12] S. Zavattoni, G. Zanganeh, A. Pedretti and M. Barbato, "High temperature thermocline TES – Effect of system pre-charging on thermal stratification," *AIP Conference Proceedings,* vol. 1734, no. 050043, 2016.

National cooperation

None

International cooperation

None

Evaluation 2017 and outlook for 2018

The majority of planned tasks for 2017 were completed according to the project time schedule. However, a delay in some of the activities was registered during the year and, in agreement with BFE, all the originally declared project objectives will be reached.